AgRP Neuron Activity Predicts and Tracks the Glycemic Response to Oral Glucose

Micaela Glat[1], Anna J. Bowen[1], Yang Gou[1], Elizabeth Giering[1,3], Jarrad M. Scarlett[1,2], Gregory J. Morton[1], and Michael W. Schwartz[1]

[1] University of Washington Medicine Diabetes Institute, Department of Medicine, Seattle, WA, 98109, USA.

[2] Department of Pediatric Gastroenterology and Hepatology, Seattle Children's Hospital, Seattle, WA, 98145, USA.

[3] Veterans Affairs Puget Sound Health Care System, Seattle, WA, 98108, USA.

Authorship note: MG and AB are co-first authors.

Conflict of interest: Funding in support of these studies was provided to M.W.S. through an agreement with Novo Nordisk (CMS-431104).

Corresponding author

Michael W. Schwartz, MD
University of Washington Medicine Diabetes Institute, Department of Medicine
750 Republican St Box 358055
Seattle, Washington, 98195, USA.
Phone: +1 (206) 897 5288
Email: mschwart@uw.edu

Abstract

Hypothalamic AgRP neurons are uniquely responsive to nutritional cues and play important roles in fuel homeostasis. To investigate how their activity is coupled to the glycemic response to an oral glucose load, we simultaneously monitored AgRP neuron activity (by fiber photometry in AgRP-IRES-cre mice) and the arterial glucose level, both before and after oral gavage (OG) of either water or glucose (0.5-2.5 g/kg). We report that the AgRP neuron response to OG glucose can be subdivided into two functionally distinct phases – one that begins prior to glucose delivery and a second that extends from peak inhibition through the return towards baseline. The 'first phase' appears to be anticipatory in nature and is also predictive of subsequent changes in glycemia, suggesting a role in the handling of an oral glucose load. To facilitate analysis of the second phase, we employed a model that allows residual activity to be removed subsequent to the 'first phase' component. This analysis reveals that the degree of residual inhibition tracks the glycemic response, and is temporally aligned with the BG rate of change (which is predictive of future BG levels), with AgRP neurons lagging BG rate of change by ~5 minutes. We conclude that the AgRP neuron response to an oral glucose challenge consists of two distinct phases, each with its own determinants and metabolic implications: an initial anticipatory component that is predictive of the subsequent glycemic response, and a second phase that is shaped by the rate of BG change.

1. Introduction

The glycemic excursion following an oral glucose load is maintained within narrow physiological limits by dynamic and highly integrated interactions across central and peripheral tissues throughout the body [1]. Contributing factors include the rate of gastric emptying, the secretion of incretin peptides (such as glucagon-like peptide-1 (GLP-1) and gastric inhibitory polypeptide (GIP)) from intestinal enteroendocrine cells, and the secretion of insulin in response to nutrient stimuli [2–4]. In addition, 'gut-brain' signals transmitted by vagal and somatosensory afferent neurons also convey changes of nutritional state from the gastrointestinal (GI) tract to the brain, and the brain in turn mounts autonomic and neuroendocrine responses that shape glucose handling [5,6]. Importantly, some of these responses are mounted before nutrient ingestion, in anticipation of the coming nutrient load [4].

Neurons located in the hypothalamus play key roles in this control system. Among the best-studied of these are AgRP neurons, situated in the hypothalamic arcuate nucleus (ARC) [7]. These neurons are activated by fasting [8], uncontrolled diabetes [9,10], and other fuel-depleted states, and this activation response is rapidly reversed by nutrient presentation [11–13]. These neurons are inhibited not only by consuming food, but by infusion of macronutrients directly into the GI tract [7], or even by the sight or smell of food [7,13,14].

These observations highlight how AgRP neuron activity is regulated not only by changing nutritional status, but by the anticipation that nutritional status will soon change. Relevant nutrient-related cues that can impact these neurons include gut-brain signals, hormones such as insulin, leptin and ghrelin, and circulating nutrients such as glucose [12,15,16]. Further, AgRP neurons are activated in most forms of diabetes [7,17–19], and we recently reported that in a mouse model of type 2 diabetes, hyperglycemia can be normalized by silencing these neurons, despite having no effect on food intake or body weight [17].

Such observations add salience to the question of how AgRP neuron activity and changing BG levels are coupled to one another. To address this question, we simultaneously monitored AgRP neuron activity (by fiber photometry) and the arterial BG level (by continuous glucose monitoring (CGM)) in 5-hour fasted mice. Data were collected both prior to and after oral gavage (OG) of either water or one of four doses of glucose (0.5-2.5 g/kg), and computational modeling was employed to quantify these relationships.

We report that the AgRP neuron response to OG glucose can be subdivided into two distinct components. The first of these comprises a rapid inhibitory phase that begins prior to glucose delivery, suggestive of an anticipatory response, and it appears to help to shape the ensuing glycemic excursion. Following a brief transitional period during which peak neuronal inhibition occurs, the 'second phase' of the response (during which AgRP neuron activity returns towards its baseline value) appears to be shaped by the glycemic excursion – specifically, the BG *rate of change*. Collectively, these observations highlight the complex, multiphasic relationship between AgRP neuron activity and the glycemic response to an oral glucose load.

2. Results

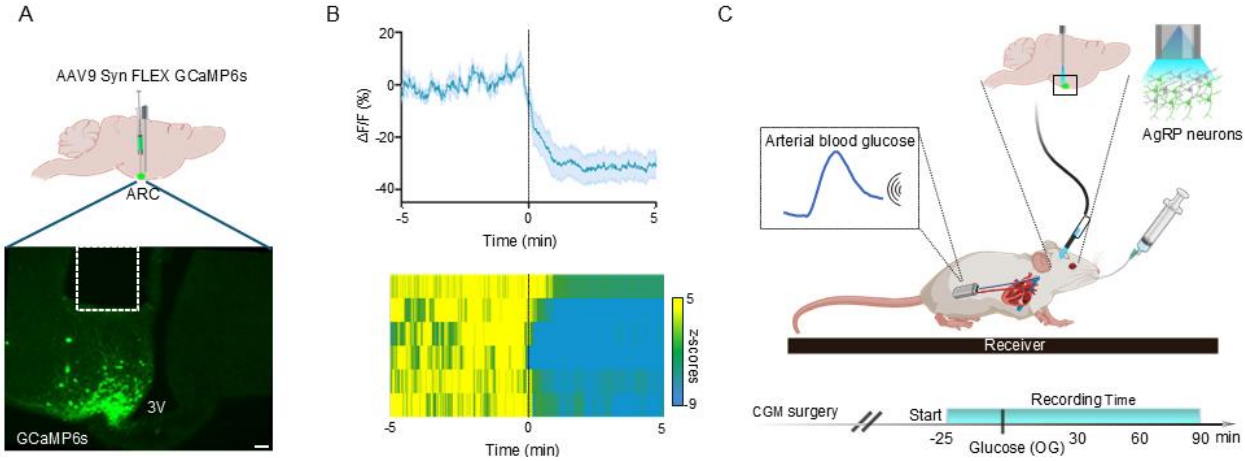

Figure 1. Experimental setup and validation of calcium activity response in AgRP neurons in vivo.
(A) Schematic of viral injection and optic implant placement for photometry recordings of AgRP neuron activity (top), and representative image of GCaMP6s expression in the ARC (bottom; scale bar = 200 μm). (B) GCaMP6s responses to chow presentation (time = 0 min) in overnight-fasted AgRP-IRES-Cre mice (n = 6); mean ± SEM (top) and heat map of z-scored activity for individual mice (bottom). (C) Experimental design for simultaneous photometry and continuous glucose monitoring (CGM) in 5-hour fasted mice receiving glucose via oral gavage (OG).

2.1 To identify relationships between AgRP neuron activity and the blood glucose level following an oral glucose load, we combined fiber photometry (FP) with continuous arterial glucose monitoring (CGM). AgRP neuron-specific expression of a Cre-dependent AAV encoding the calcium reporter GCaMP6s (Fig. 1A) was confirmed both by observing rapid AgRP neuron inhibition following chow presentation to overnight-fasted mice (Figure 1B) and by postmortem detection of GCaMP6s expression in AgRP neurons (Figure 1A). Either water or one of 4 doses of glucose (0.5, 1.0, 2.0, and 2.5 g/kg) was administered via the OG route in separate sessions. Monitoring commenced 25 min before OG administration and was maintained for 90 min thereafter, with dose order randomized across days. Prior to data analysis, CGM traces were processed with robust despiking, median filtering, and causal smoothing, then baseline-subtracted to yield the change of glucose over time (ΔG(t); see Methods, Glucose analysis).

As expected, oral glucose elicited an increase of the BG level that was dose-dependent with consistent temporal dynamics across sessions. Both the peak BG change from baseline (peak ΔG) and rate of BG rise increased in a dose-dependent manner (Figure 2A-E). Because the rate of BG decline after the peak was also proportional to the OG glucose dose, overall recovery times were similar irrespective of dose (Figure 2F). Consequently, while peak ΔG and the rates of rise and fall of BG were strongly dose-correlated (R^2 = 0.38, 0.34, and 0.46, respectively), the incremental area under the blood glucose curve (iAUC) was not (R^2 = 0.18) (Figure 2D-G).

2.2 Processing of Z-scored FP signals from AgRP neurons in parallel with glucose traces (see Methods, Fiber photometry analysis) reveals that as expected [12,16], the activity of these neurons was markedly and rapidly decreased by OG glucose administration and remained suppressed for tens of minutes as the plasma BG levels rose and then subsequently declined. Closer inspection of individual traces showed that in most cases, however, AgRP neuronal activity began to decline from its baseline *prior to* OG delivery itself (Figure 2H). This interpretation was

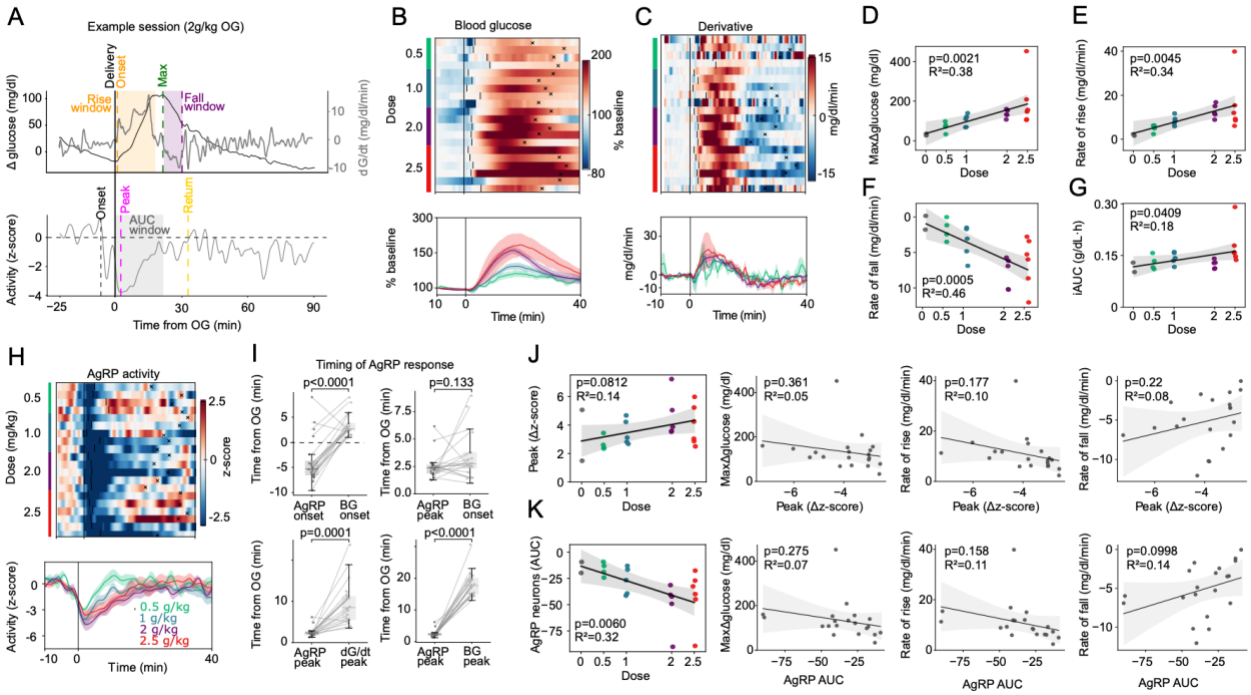

Figure 2. AgRP neuron responses to varying doses of oral glucose.
(A) Example session showing blood glucose (BG) dynamics (top) and AgRP neuron activity (bottom) following OG of 2 g/kg glucose. (B) Heat-map of baseline-normalized BG levels for individual mice receiving different glucose doses (0.5–2.5 g/kg) over 40 minutes. Vertical lines mark the time of rise; x-marks indicate the time of return to half-maximum (top). The lower panel shows dose-averaged baseline-normalized BG. (C) Heat-map of BG derivatives after varying glucose doses, with time of rise and return to half-maximum indicated as in (B) (top). The lower panel shows mean BG derivatives for each dose group. (D–G) Correlation between glucose dose and: peak ΔBG (D), BG rate of rise (E), BG rate of fall (F), and incremental area under the curve (iAUC) over 1 h after glucose or water administration (G). (n = 2–6 per group). (H) Heat-map of AgRP neuron activity following different glucose doses, with rise onset and time of return to half-maximum indicated (top). The lower panel shows mean activity for each dose. (n = 4–6 per group). (I), Timing of AgRP neuron responses relative to BG dynamics: time of inhibition onset and inhibition peak compared to BG onset (top panels), and time of AgRP peak inhibition compared to time of peak BG derivative (bottom left) and peak BG (bottom right). (J) Correlations between peak AgRP inhibition (Δz-score, 0–10 min after OG) and glucose dose (first panel), as well as peak BG, BG rate of rise, and BG rate of fall (second–fourth panels). K, Correlations between negative AUC of AgRP responses (t = 0 min to peak BG) and glucose dose (first panel) or BG metrics (peak ΔBG, rate of rise, and rate of fall; second–fourth panels). Statistical comparisons between groups were performed using Wilcoxon tests (J), and correlations in (D-G and J–K) were assessed using ordinary least squares (OLS) linear regression with subject fixed-effects; shaded regions represent slope 95% confidence intervals.

confirmed by aligning AgRP neuronal activity recordings to the time of OG administration (AgRP neuron inhibition onset = -5 min vs BG onset = 1 min, p = 0.00071, and AgRP neuron peak inhibition = 2 min vs peak dG/dt = 8 min, p = 0.0001; Fig. 2i left panel).

We then considered whether this earliest AgRP neuronal response ('first phase') reflects an anticipatory response conditioned by prior glucose exposures. In support of this hypothesis, the onset of AgRP neuronal inhibition occurred earlier among mice receiving their second glucose bolus compared to their first (Supplementary Figure S1A), suggesting a learned component. Additionally, an inhibition was detected when water was administered (instead of glucose) following prior glucose exposures (Supplementary Figure S1B). In contrast, this response was not observed when either water or glucose was given as the first OG administration (Supplementary Figure S1C). Thus, this 'first phase' decrease of AgRP neuronal activity appears to be a learned, anticipatory response.

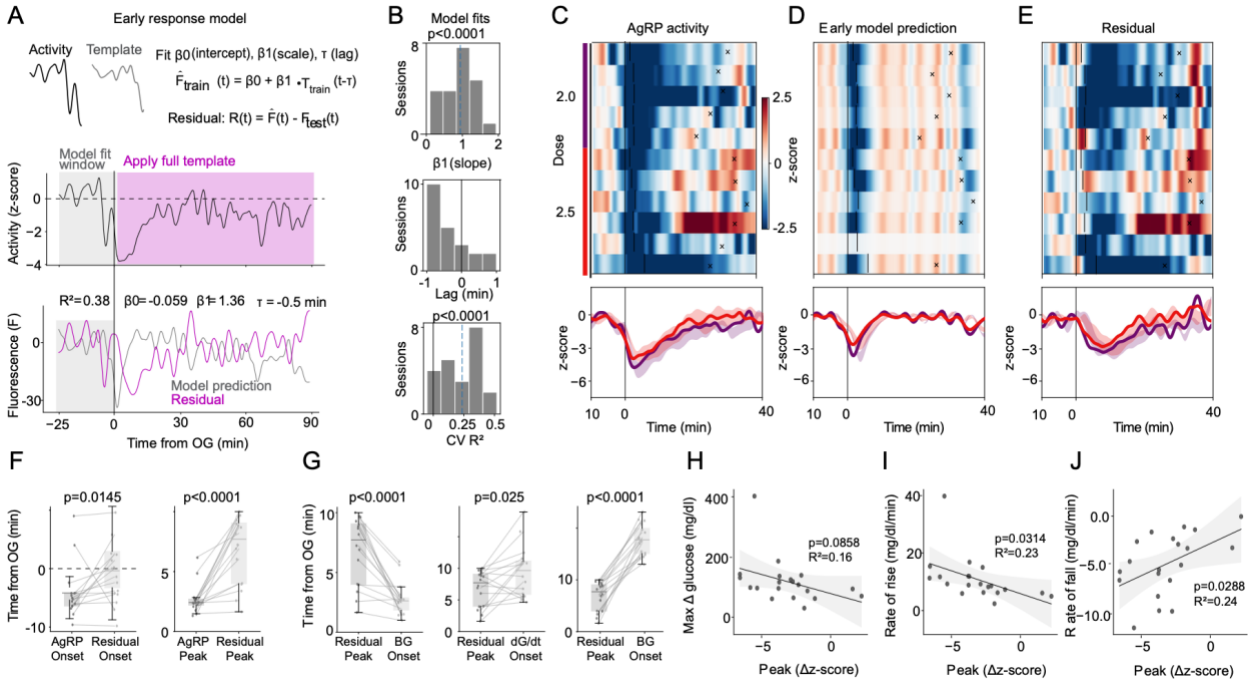

Figure 3. Dissocation between phase 1 and phase 2 responses using an early-response model.
(A) Early-response model (see methods) illustrating the cross-validated prediction $\hat{F}_i(t)$ generated from low-dose (0 and 0.5 g/kg) sessions and the corresponding residual trace $R_i(t) = F_i(t) - \hat{F}_i(t)$, representing activity exceeding the early template (top). The middle panel shows AgRP neuron activity (z-score) used to fit the model window (−25 to +1 min) and the post-absorptive glucose template. The bottom panel displays the model prediction separated from the residual component. (B) Histograms showing early-response model fits across sessions: slope (top), lag (middle) and cross-validated R^2 (bottom). (C-E) Heat-maps (top) and mean AgRP neuron activity (bottom) for the original (C), cross-validated prediction (D), and residual (E) traces in mice administered 2 or 2.5 g/kg glucose. (F) Timing of AgRP neuron responses: comparison of onset inhibition (left) and peak inhibition (right) before vs after model decomposition (residual). (G)**,** Timing of AgRP neuron peak inhibition after correction: comparison with time of BG rise (left), BG peak derivative (middle), and BG peak (right). (H-J) Correlations between corrected AgRP neuron responses and BG metrics: peak ΔBG (H), BG rate of rise (I), and BG rate of fall (J). Statistical comparisons between groups were performed using the Wilcoxon tests (F and J). Correlations in (H–J) were assessed using ordinary least squares (OLS) linear regression with fixed effects for subject; shaded regions indicate slope 95% confidence intervals.

Peak AgRP neuronal inhibition following OG glucose coincided with the onset of rising BG levels (Figure 2I, right panel), but unexpectedly, its magnitude (captured by the peak negative z-score in a 0-10 min window following glucose administration) was invariant. Stated differently, peak inhibition did not vary with glucose dose, peak BG, or either the rate of rise or rate of fall of BG (Figure 2J), indicating a largely stereotyped, administration-aligned population response whose amplitude is largely independent of either the amount of oral glucose given or the subsequent glycemic response. Consistent with this early-phase dissociation, the broader suppression of AgRP neuron activity measured by incremental area under the curve (iAUC) from delivery (t=0) to time of peak plasma BG likewise showed no meaningful relationship to post-absorptive BG metrics (Figure 2K; see Supplement for iAUC analyses), despite varying with glucose dose.

2.3 To investigate the relationship between the glycemic excursion and AgRP neuron activity subsequent to its rapid initial decline (which includes the last phase of AgRP neuronal inhibition and its subsequent recovery towards its baseline, referred to herein as the 'second phase' response), we developed a model that isolates second phase activity from the first phase. (Figure 3A, see Methods, Early-response model).

We fit the model's lag and scale parameters using only the pre/early window (−20 to +1 min relative to glucose delivery) from glucose-administration sessions, optimizing these parameters within inner cross-validation folds (see Methods, Early-response model). We then applied the resulting early-response prediction to a held-out low-dose test set (0 and 0.5 g/kg) and quantified deviations in the post-administration period (time points never used for fitting) as residuals, $R_i(t) = F_i(t) - \hat{F}_i(t)$. In this framework, residuals provide a session-by-session estimate of late activity not explained by the initial, BG-trajectory–independent, stimulus-locked component: the more the second phase is shaped by the glycemic response, the larger (more negative) the deviation from the early-model prediction.

Consistent with this decomposition, the early-response model closely captured the rapid initial decrease in AgRP neuronal activity, but it did not account for the sustained suppression that followed at higher glucose doses. Residuals became increasingly negative over time, peaking several minutes after BG began to rise, before gradually returning toward baseline (Figure 3B). Population heatmaps of the original, fitted, and residual traces confirmed this decomposition. Thus, the second phase component was weak or absent at low glucose doses but emerged prominently as extended inhibitory residual structure at higher doses (2 and 2.5 g/kg, Figure 3C-E).

We next interrogated the relationships between second phase AgRP neuronal activity and both the BG change over time and *the rate of BG change* (*i.e.,* the BG derivative, which predicts the direction of future BG change). While the raw AgRP peak neuronal inhibitory response occurred concurrently with the initial rise in BG, this early response was captured by the early model, with peak inhibition in the residual now occurring later and aligning more closely with time of peak BG rise (Fig. 3f and g). Accordingly, while peak residual inhibition occurred well before the BG peak, it no longer differed from the peak of the glucose derivative (Figure 3G). Interestingly, while the degree of maximum residual inhibition remained uncorrelated with the peak ΔG, it correlated significantly with rates of BG rise and fall (R^2 = 0.23 and R^2 = 0.24, respectively; Figure 3H), suggesting that larger glycemic responses influence the second phase AgRP neuronal response. By comparison, applying the same procedure to data from mice receiving either OG water or low-dose glucose (0.5 mg/kg) produced small residuals with no consistent stimulus-aligned structure and no significant relationship to glucose dynamics (Supplementary Figure S2).

2.4 To quantify how the two phases of the AgRP neuronal response are coupled to the change in glycemia, we used lagged cross-correlation [20]. Correlations were computed over ±20 min lags and evaluated against pseudosession nulls (obtained by pairing FP with circularly shifted glucose traces; see Methods, Cross-correlation analysis). In the Early-response model FP signal, cross-correlations with BG and its derivative (based on an OG glucose dose of 2 mg/kg) were strong and skewed toward negative lags**:** the peak correlation occurred when AgRP neuron inhibition led the blood glucose signal by ~10–15 min and its derivative by ~0-10 min (Figure 4A-D), consistent with the first-phase response arising as an anticipatory signal.

After subtracting the early-response template from the raw FP signal, however, this coupling pattern changed. Residual activity remained significantly correlated with the blood glucose level,

but with somewhat lower peak magnitude (Figure 4D). Importantly, the peak cross-correlation with the glucose derivative shifted to a short positive lag of ~5 min, with residual AgRP activity following rather than preceding the glucose derivative (Figure 4C). This positive-lag trough significantly exceeded pseudosession nulls and was consistent across animals, indicating that once the early, administration-locked component is removed, the remaining activity primarily tracks the BG rate of change, rather than the BG level itself. Residual activity approached baseline near the time of peak BG (Figure 3G), consistent with an inhibitory response that begins shortly after glucose rise and relaxes as glucose levels begin to fall.

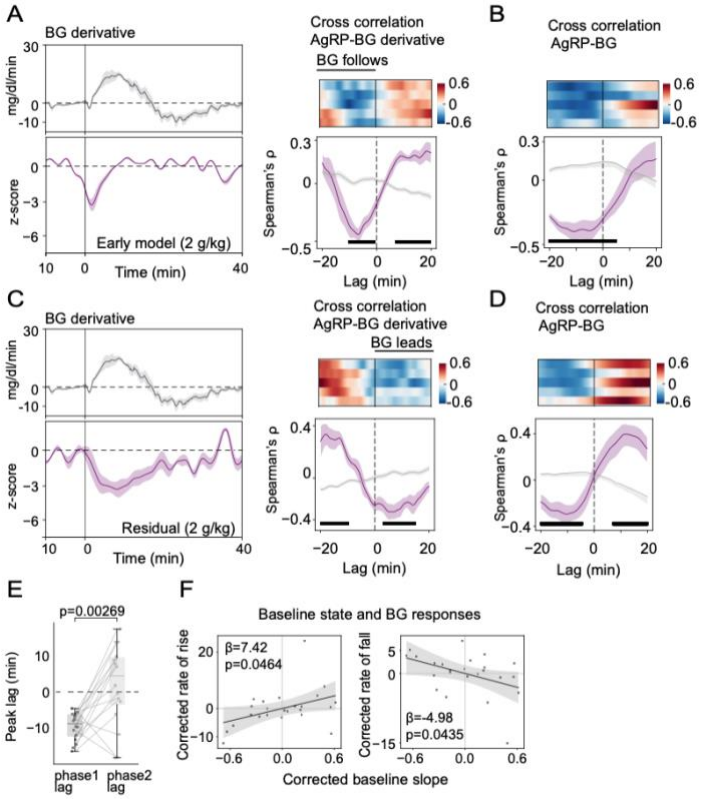

Figure 4. Temporal relationship between AgRP neuron activity and BG.
(A) Mean BG derivative (A, top) and AgRP early-model estimated activity (bottom, z-scores) after a 2 g/kg glucose dose. (A and B), Lagged cross-correlation between the early AgRP response and BG derivative (A, right) or the BG concentration (B). (C and D) Lagged cross-correlation between the residual component the BG derivative (C, right) or the BG concentration (D); vertical ticks indicate bins where $p<0.01$. Both FP and BG time series were rank-transformed (Spearman), and correlations were computed over ±20-min lags and evaluated against pseudosession-derived null distributions (Wilcoxon tests with Benjamini-Hochberg correction for multiple comparisons). (E) Comparison between peak lag before and after correction (phase 1 vs phase 2). (F) Correlations between AgRP neuron baseline state and BG rate of rise (left) or BG rate of fall (right). Slope from linear mixed effects model with corrections for dose, subject, and baseline BG level.

2.5 To quantify the extent to which baseline AgRP neuron state (prior to oral glucose delivery) predicts the subsequent glycemic response to a given glucose load, we analyzed a slope parameter generated from each session by the Early-response model. This parameter provides a measure of how strongly that session's baseline and immediate post-gavage neuron activity conform to the canonical early template (β_1 in Figure 3A). We interpreted this as a simple baseline "state" metric, where a larger slope indicates greater-than-average inhibition in the baseline and early-response periods, and vice versa.

Across sessions, greater slopes predicted increased rates of BG rate of rise and fall for a given glucose dose (Figure 4F). This finding implies that differences in pre-absorptive AgRP state contribute to trial-to-trial variability in the glycemic impact of the same nominal glucose load. A complementary baseline measure derived from the low-frequency structure of the FP signal during the pre-administration period showed a similar relationship to dose-corrected iAUC (Fig. S3), confirming that slow inhibition at baseline predicts a greater glycemic excursion with a more rapid rise and fall.

3. Discussion

In addition to their potent stimulatory effects on food intake, AgRP neurons are increasingly recognized as key regulators of glucose homeostasis [21–26]. For example, these neurons are activated in most forms of diabetes [19,27–29], and in a mouse model of type 2 diabetes, AgRP neuron hyperactivity is required for hyperglycemia, but is dispensable for hyperphagia and obesity [17]. Moreover, AgRP neurons have been described as "glucose-inhibited" based on ex vivo studies [30], and in vivo fiber photometry studies show that their activity decreases following either oral glucose or glucose infusion into the hepatic portal vein [16]. Together, these observations support a model wherein AgRP neuron hyperactivity promotes hyperglycemia, which in turn feeds back to inhibit these neurons. Accordingly, we hypothesized that following an oral glucose load, AgRP neuron activity would both be inhibited by and help to shape the glycemic response.

To test this hypothesis, we implemented a strategy wherein AgRP neuronal activity and the arterial glucose level are monitored continuously both prior to and after OG glucose administration. Computational analysis of these data reveals several novel findings. First, we show that in sessions conducted in mice previously subjected to OG glucose administration, reduced AgRP neuronal activity is detectable *before* that session's OG administration. This early inhibitory response was consistently observed across subsequent sessions, regardless of whether water or glucose was administered. Thus, this 'first phase' response appears to be mounted in anticipation of an oral glucose load. This interpretation is strengthened by the finding that neither its timing nor its magnitude is impacted by glucose dose (which, of course, cannot be anticipated).

Such an anticipatory response is analogous to the rapid AgRP neuron inhibition reported in response to the sight or smell of food, even if the food is not eaten [11,13,14]. The neurocircuitry implicated in this anticipatory AgRP neuron response appears to be distinct from that underlying the more sustained inhibition induced by food ingestion. Specifically, AgRP neuron inhibition by sensory cues involves projections from the lateral hypothalamic area to inhibitory GABAergic neurons in the dorsomedial hypothalamus (DMH) that lie upstream of and inhibit AgRP neurons [31]. Additional studies are warranted to determine whether this pathway also underlies the anticipatory 'first phase' response reported here, and the extent to which this early response carries information about both the animal's expectation and its internal state before ingested nutrients are absorbed.

That the early decrease of AgRP neuron activity *1)* precedes OG glucose delivery, *2)* appears to be anticipatory in nature, and *3)* is predictive of the glycemic excursion (*i.e.,* greater early inhibition predicts better glucose tolerance) raises a series of questions. Is it possible, for example, that early AgRP neuron suppression participates in cephalic phase/autonomic control of glucose handling? Such a response can clearly influence gastric emptying, intestinal transit, insulin secretion, and hepatic glucose output, and is supported by evidence that elevating AgRP activity impairs hepatic insulin sensitivity and increases hepatic glucose production [32]. An alternative (and non-mutually exclusive) explanation is that early AgRP neuron suppression primarily reports internal state (e.g., hunger/arousal): sessions starting from a higher hunger-related AgRP neuron

activity baseline may exhibit larger early inhibition and, independently, altered GI absorption and clearance dynamics. Thus, while early AgRP dynamics are predictive of glycemic responses, establishing whether this reflects a causal role for AgRP neurons versus shared upstream, state-dependent control will require targeted manipulations and direct measurements of intermediate physiological steps.

Following the 'first phase' inhibitory response and the subsequent transition period during which inhibition peaks, AgRP neuron activity gradually rises towards its baseline level. Unlike the first phase response, this 'second phase' is consistently associated with BG metrics. To optimize the analysis of this relationship, we constructed a model wherein the 'first phase' response is effectively subtracted to reveal the second phase. This analysis showed that during the second phase, slower recovery of AgRP neuron activity (greater inhibition) is associated with more rapid rates of BG rise and fall. Interestingly, the second phase response dynamics aligned more closely with the BG *rate of change* (derivative) than with the absolute BG level. This observation parallels the finding that following an oral glucose load, hypothalamic orexin neuron activity and BG rate of change are tightly linked to one another [33]. Since the rate of change of a parameter is more predictive of future state than its absolute value, sensory detection of rate of change aligns with an 'allostatic' control mechanism that combines interoceptive processing with learned experience to mount anticipatory responses based on predictions about future state [34,35].

Taken together, these findings demonstrate that the AgRP neuron response to oral glucose comprises two functionally distinct phases, each with their own unique relationship to the glycemic response. The first phase, stimulus-aligned component (captured by a simple, BG-trajectory**–** independent template) predicts how a given glucose load will impact the subsequent glycemic response. While additional studies are needed, we interpret these findings to suggest that AgRP neurons transduce anticipatory information about impending nutrient delivery into adaptive metabolic responses that optimize glucose handling. Subsequent to this first phase is a second phase that *1)* remains after template subtraction, *2)* scales with dose-dependent BG metrics**,** and *3)* is coupled to BG dynamics – in particular, the rate of BG change. These findings lay the foundation for future investigation into whether the relationship exist between AgRP neurons and other circulating macronutrients resembles that we have documented with glucose. An additional priority is to determine if relationships between AgRP neuron activity, glucose ingestion, and homeostatic control of glycemia are altered in obesity, diabetes, and related metabolic disorders.

4. Methods

4.1 Animal Studies.

All animal experiments were conducted in accordance with the National Institutes of Health Guide for the Care and Use of Laboratory Animals, and all procedures were approved by the Institutional Animal Care and Use Committee at the University of Washington, Seattle, WA. AgRP-IRES-Cre mice (kindly provided to us by Dr. Streamson Chua, Jr (Albert Einstein College of Medicine) have previously been described [36] and are readily available from Jackson Laboratories (012899, Bar Harbor, ME, USA). Mice were individually housed in a temperature-controlled room on a 14:10 light:dark cycle under specific pathogen-free conditions with ad libitum access to drinking water and standard laboratory chow (PMI Nutrition, St. Louis, MO). Before experimental sessions, mice were fasted for either 16 h (for validation studies) or for 5 h (for analysis of the relationship between AgRP neuron activity and the BG level), as detailed in the text and figure legends.

4.2 Surgeries.

To measure AgRP neuron activity, we stereotaxically injected unilaterally into the ARC (anterior-posterior (AP), -1.5 mm; mediolateral (ML), 0.3 mm; dorsoventral (DV, from dura), -5.85 mm, 400 nl, at a rate of 100 nl/min) an AAV containing a cre-inducible GCaMP6s cassette: pAAV9-CAG-FLEX-GCaMP6s (Addgene, Plasmid no. 100842, Watertown, MA, USA, titer $1X10^{13}$ per ml) into AgRP-IRES-Cre mice as previously described [37,38]. In the same surgery, a photometry cannula (MFC_400/430–0.48_6.1 mm_MF1.25_FLT, Doric Lenses, Franquet, Quebec, Canada) was implanted above the injection site (AP = −1.5 mm, ML = −0.3 mm, DV = −5.8 mm), as described [38,39]. Mice were allowed 2–3 wk for viral expression and recovery before FP recording sessions. Accurate viral targeting and fiber placement were verified by measuring AgRP neuron responses to chow refeeding after overnight fasting. Animals showing less than ΔF/F 20% response to chow were excluded from further experiments. Accurate targeting was also confirmed at the end of each experiment by histochemical detection of GCaMP6s and optic fiber placement.

Glucose sensors (Data Sciences International (DSI), St. Paul, MN, USA) were implanted through the left carotid artery of AgRP-IRES-Cre mice following the manufacturer's guidelines and as previously described [20,40]with support of the NIDDK-funded Diabetes Research Center Metabolic and Cellular Phenotyping Core at the University of Washington. Mice were allowed 1 wk for recovery from surgery.

4.3 Fiber photometry.

AgRP neuron activity was measured using a photometry processor (RZ 10X, Tucker-Davis Technologies (TDT), Alachua, Florida, USA) as previously described [20,37,38]. Briefly, two excitation LEDs were used for this study, 405 nm at 210 Hz and 465 nm at 330 Hz, power of 30-50 μW at the implant fiber tip. These LEDs were delivered to a filtered minicube (Doric Lenses, Franquet, Quebec, Canada) and passed through patch cords (MFP_400/430/1100–0.57_0.45m_FCM-MF1.25_LAF, Doric Lenses, Franquet, Quebec, Canada) to the mouse

photometry cannulae. The 405-nm LED was used as an isosbestic signal to control for movement and photobleaching. Digital signals were collected through the processor (RZ 10X, TDT), and data were captured using the software Synapse (TDT) and analyzed using custom Python code.

4.4 Continuous arterial glucose monitoring.

HD-XG telemetry system (DSI, St. Paul, MN, USA) was used to continuously monitor blood glucose concentrations. Calibration of the implants was performed by OGTT test following the manufacturer's instructions. CGM data was acquired by Ponemah software (DSI). For data synchronization, Synapse software generated TTL pulses that were sent to Ponemah via a signal interface box (DSI), allowing alignment of FP and CGM data acquisition. Data was sampled at 1 HZ.

4.5 Study protocols.

Starting at the beginning of the light cycle, mice were subjected to a 5-h fast while remaining in their home cages. They were then connected to a patch cord for FP recordings and simultaneously placed on a receiver plate (DSI) for CGM. After a 20-min acclimation period, simultaneous FP and CGM recordings were initiated. The protocol began with baseline recordings for 25 min prior to OG administration of either water or one of four doses of glucose (0.5, 1, 2, and 2.5 g/kg). Each animal received each intervention in randomized order, and recordings continued for an additional 90 min post-gavage. For data analysis, the time of OG administration was defined as zero.

4.6 Data and statistical analysis.

Glucose analysis: Pre-processing (filtering, smoothing, baseline-subtracting). We first cleaned each glucose trace to remove artifacts while preserving timing. Obvious spikes were flagged using a robust median absolute deviation (MAD) rule ($|y-\text{median}| > k\cdot\text{MAD}$ with k = 2.0) and replaced by linear interpolation; this step eliminates transient sensor glitches without flattening true transitions. We then applied a short centered median filter (7 samples = 7 s) to suppress any remaining impulsive noise, followed by a causal moving average (60 samples = 60 s) that smooths high-frequency jitter yet keeps the response aligned in time. Finally, we defined a stable baseline from the pre-event period (−25 to 0 min from glucose administration) and worked with the baseline-subtracted signal, $\Delta G(t)$, so amplitudes are comparable across sessions.

To quantify dynamics, we computed a finite-difference derivative at 1-s spacing and smoothed it with the same 60-sample causal window**.** The response onset is the first sustained moment after t = 0 when either the derivative rises above a robust baseline threshold or the level clears a baseline-scaled threshold, with a ≥1 min sustain to avoid false starts (see below). We located the peak level of $\Delta G(t)$ within 0–90 min and recorded the peak derivative in the early window (0–30 min after glucose delivery) to capture the time and level of sharpest rise. Recovery was summarized by the half-max time (first crossing back to the baseline + 50% of peak, computed on the raw series with linear interpolation). We defined a plateau phase where the smoothed

derivative dropped into a near-zero band scaled to the preceding rise, then identified the return to baseline either by amplitude (first $\Delta G(t) \leq 0$) or by a sustained relaxation of the derivative back above a negative threshold. Overall exposure was captured by a positive-only incremental area under the curve (iAUC) over the entire post-delivery period (0–90 min), ensuring that only excursions above baseline contribute.

The first sustained rise in the BG level after t = 0 was identified by testing two independent conditions against robust, baseline-derived thresholds and requiring ≥1 min of continuous evidence (1 Hz → 60 consecutive samples). First, we smoothed the baseline-subtracted glucose $y_0(t) = G(t) - median_{[-5,0]}G$ with a 2-min causal boxcar (≈120 samples at 1 Hz) and took a finite-difference derivative dy/dt. On the baseline segment (t < 0), we computed robust centers and scales:

- **Derivative (slope) threshold.** Let d_{pre}be baseline derivatives. With median m_d and scaled MAD $\hat{\sigma}_d = 1.4826 \cdot MAD(d_{pre})$, the slope threshold is

$$T_{slope} \ = \ m_d \ + \ z\,\hat{\sigma}_d, z = 3.$$

- **Level (amplitude) threshold.** Let $y_{0,pre}$ be baseline values of y_0. With scaled MAD $\hat{\sigma}_y = 1.4826 \cdot MAD(y_{0,pre})$, the level threshold is

$$T_{level} \ = \ 3\,\hat{\sigma}_y,$$

We then mark samples $t \geq 0$ where either $\frac{dy}{dt} > T_{slope}$ **or** $y_0(t) > T_{level}$. Using a sliding window, we require this condition to hold for a continuous 1-min run before declaring onset; the onset time θ is the first sample meeting that sustain criterion.

4.7 Fiber photometry analysis.

Post-processing. Photometry data were analyzed using custom Python scripts (https://github.com/nikhayes/fibphoflow). We removed shared motion/bleaching components from raw fluorescence data by regressing a reference (isosbestic) or drift proxy onto the signal channel and subtracting the fitted component. This targets very slow, non-neural trends so the remaining signal reflects neural activity more faithfully.

Pre-processing (median, causal smoothing, low-pass, z-score).

Photometry signals received the same robust clean-up as glucose: MAD-based de-spiking (k = 2.0), then a centered median filter (7 samples) to eliminate outliers without blurring edges. We followed with a causal moving average (60 samples) so short-latency features remain time-aligned. To further suppress slow, noninformative fluctuations, we applied a zero-phase Butterworth low-pass defined by period (cutoff 4 min, order 3); framing the cutoff in minutes makes

settings consistent across sessions at 1 Hz. For comparability across animals, we **z-scored** each trace within the baseline (−25 to 0 min), yielding $Z_{FP}(t)$ with mean 0 and unit SD at baseline.

Response metrics.

*Onset of low-frequency activity***.** We quantified response timing by tracking when low-frequency photometry power arose around glucose delivery. For each session, we computed a spectrogram of the baseline-z-scored trace $Z_{FP}(t)$ using 15-min windows with 99% overlap. This yielded power spectral density $S(f,\tau)$ in cycles per minute (cpm) as a function of time τ relative to the event. We focused on a single low-frequency band corresponding to periods between 14 and 20 minutes,

$$f \in [1/20,\ 1/14] \approx [0.05,\ 0.071]\, cpm,$$

and retained only frequencies in this range. Band-limited power at each time bin was defined as

$$P_{real}(\tau) = \frac{1}{|\ B\ |}\sum_{f\in B} S_{real}(f,\tau)$$

where B indexes the 14–20 min band. To test whether this power exceeded chance within the same session, we constructed a jittered null using pseudo-events. We drew $N \approx 200$ pseudo-onset times, excluding a 5-min guard around the true glucose time. For each pseudo-event, we repeated the same segmentation and band-limited spectrogram, giving null band-power traces $P_{null}^{(k)}(\tau)$. At each time bin we then computed an upper-tailed, rank-based p-value:

$$p(\tau) = \frac{1 + \#\{k: P_{null}^{(k)}(\tau) \geq P_{real}(\tau)\}}{N+1},$$

so that small $p(\tau)$ indicates that observed band power exceeds the null. We restricted detection to the symmetric window from −10 to +10 min around glucose delivery. The frequency-specific response onset time was defined as the first-time bin $\tau^* \in [-10,10]$ where band power significantly exceeded the null. Sessions without any bin meeting this criterion were classified as having no detectable response in the 14–20 min (≈0.05–0.071 cpm) band.

Baseline low-frequency power (PSD slope). Within the baseline window we estimate Welch's power spectral density (PSD) and fit a simple aperiodic $1/f^k$ model in log–log space. The slope k summarizes bias towards slow baseline structure (higher slope greater low-frequency bias). *Peak z-response.* In an early window (0–15 min) we report the maximal Z_{FP}. This captures the sharpest early deflection relative to baseline variability.

4.8 Area under the curve (AUC).

We compute an incremental AUC from glucose delivery (t = 0) to the time of peak blood glucose using NumPy's trapezoidal rule, after setting all values above baseline to 0; this integral therefore reflects only negative deflections**.** We also compute a total AUC from t = 0 to the end of the

session using the unmodified signal (no clipping), providing an overall measure of deviation from baseline.

4.9 Early-response model.

To isolate stereotyped early, dose-agnostic dynamics from putative feedback components, we fit a simple lagged linear model only on pre-response activity and then examine residuals predicted from held-out sessions.

Model and variables. Let $F_i(t)$be the z-scored FP for session i, and let $F^{-}_{train}(t)$ be a **template** formed by averaging the baseline-aligned FP across the *training* sessions (see below). For a candidate lag $\tau \in [-1{:}\,0.25{:}\,1]$ minutes, we fit

$$\hat{F}_i(t;\tau) \;=\; \beta_0 \;+\; \beta_1\, F^{-}_{train}(t-\tau),$$

$$t \in [-25,\, +1]\; min,$$

with β_0 (intercept), β_1 (slope/scale), and τ (temporal offset). Parameters $\beta_0, \beta_1$are estimated by ordinary least squares for each τ; τ is chosen by inner-fold cross-validation (below). This "template-regression" captures how strongly each session follows the average early pattern, while allowing a small temporal shift.

Training set, template construction, and test set. Training data comprised oral glucose sessions at 1.0, 2.0, and 2.5 mg/kg. For each session, we extracted the pre-peak window (−25-+1 min relative to the event) and resampled on the native 1 Hz grid. The template $F^{-}_{train}(t)$ was computed as the across-session median at each time point to be robust to outliers. The test set consisted of water and 0.5 mg/kg sessions, held out entirely during model selection.

Inner-fold cross-validation (model selection). We performed K-fold cross-validation (CV) across *training sessions* (folds stratified by subject when possible). For each candidate lag τ (e.g., a small grid around zero), we:

1. Rebuilt $F^{-(-k)}_{train}(t)$ from the K−1 training folds (leaving fold *k* out).
2. Fit β_0, β_1on those folds by minimizing squared error on $t \in [-25, +1]$min.
3. Predicted the left-out fold using $\hat{F}_i^{(-k)}(t;\tau)$and accumulated validation error.

We selected $\tau^{\backslash *}$that minimized average validation mean-squared error (MSE) (tie-break by higher R^2), then refit β_0, β_1on all training sessions using the template built from **all** training data and the chosen lag $\tau^{\backslash *}$.

Evaluation on held-out sessions and residuals. With $\tau^{\backslash *}$and (β_0, β_1) fixed, we generated predictions $\hat{F}_i(t;\tau^{\backslash *})$ for each session from held-out averaged activity on water/0.5 mg/kg sessions. We then computed residual FP

$$R_i(t) \;=\; F_i(t) \;-\; \hat{F}_i(t;\tau^{\backslash *}).$$

Because the model is fit exclusively on pre-peak-response activity and predictions are generated from low-dose glucose sessions**,** these residuals emphasize deviations that cannot be explained by the dose-agnostic early pattern that dominates low-dose glucose responses, including feedback-like components or dose-sensitive dynamics. For summary displays and statistics, we aggregated residuals over analysis windows (e.g., 0–10 min early, 10–60 min late) and, when needed, averaged across held-out sessions to visualize the typical "beyond-early-phase" deviation profile.

4.9 Cross-correlation analysis (Spearman, nulls, aggregation).

To characterize FP–glucose coupling and residual FP-glucose coupling without assuming linearity, we rank-transformed both series (Spearman) and computed lagged correlations over ±20 min in 1 s steps. We assessed specificity with pseudosession nulls generated by pairing FP with circular shifts of other sessions' glucose (with a minimum 20 min offset). For group summaries, we Fisher-transformed per-session correlations, averaged in z-space (which stabilizes variance), mapped back to ρ for plotting, and controlled multiple comparisons across lags using a Benjamini-Hochberg correction for multiple comparisons.

4.10 Implementation notes.

All data were sampled at 1 Hz. All analyses were implemented in Python using NumPy/Pandas for array and table operations, SciPy for filtering and frequency-based analysis (Savitzky–Golay, Butterworth/filtfilt, Welch PSD, spectrogram), scikit-learn for linear modeling, and Matplotlib for figures. All configurable parameters (windows, orders, thresholds, lags, null counts) are exposed via MetricsConfig (glucose) and FPConfig (photometry) and are reported with the results to support full replication.

4.11 Data and materials availability

All data are available at: https://doi.org/10.6084/m9.figshare.31891579. A detailed data description and companion code are at: https://github.com/thebowenlab/glucose-photometry.git

AUTHORSHIP NOTE. MG and AB are co-first authors

ACKNOWLEDGMENT. The authors appreciate the technical assistance studies provided by Dr. Michael Bruchas, University of Washington, and Lisa Beutler and Nikolas Hayes (Northwestern University) for in vivo fiber photometry studies and analysis including custom scripts, and mouse colony management by Vincent Damian at the University of Washington.

AUTHORSHIP CONTRIBUTION STATEMENT. Micaela Glat: Writing review & editing, Writing original draft, Supervision, Resources, Project administration, Methodology, Investigation, Formal analysis, Data curation, Conceptualization. **Anna J. Bowen:** Writing review & editing, Writing original draft, Supervision, Resources, Project administration, Methodology, Investigation, Funding acquisition, Formal analysis, Data curation, Conceptualization. **Yang Gou:** Methodology, Investigation, Data curation, Conceptualization. **Elizabeth Giering:** Methodology, Investigation.

Jarrad M. Scarlett: Writing review & editing, Writing original draft, Resources, Project administration, Conceptualization. **Gregory J. Morton:** Writing review & editing, Writing original draft, Resources, Project administration, Conceptualization. **Michael W. Schwartz:** Writing review & editing, Writing original draft, Supervision, Resources, Project administration, Methodology, Investigation, Formal analysis, Data curation, Conceptualization.

DECLARATION OF COMPETING INTERESTS.

The authors declare the following financial interests/personal relationships which may be considered as potential competing interests: Michael W. Schwartz reports financial support was provided by National Institute of Diabetes and Digestive and Kidney Diseases. Jarrad Scarlett reports financial support provided by National Institute of Diabetes and Digestive and Kidney Diseases and the US Department of Defense. Gregory Morton reports financial support was provided by National Institute of Diabetes and Digestive and Kidney Diseases. Michael Schwartz reports a relationship with Novo Nordisk Inc that includes: funding grants.

FUNDING

This work was supported by grants to: M.W.S. (NIDDK Grants DK083042 and DK101997), Y.G. (Cystic Fibrosis Foundation SINGH19R0 and SINGH24R0), J.M.S. (NIDDK Grants K08 DK114474, R03 DK128383, and DoD W81XWH2110635), G.J.M. (R01 DK089056, and R01 DK124238), A.B (Howard Hughes Medical Institute Hanna H. Gray Fellowship), the NIDDK-funded Nutrition Obesity Research Center (DK035816), and the NIDDK-funded Diabetes Research Center (DK017047) at the University of Washington. Funding in support of these studies was also provided to M.W.S. through an agreement with Novo Nordisk (CMS-431104).

Supplemental figures

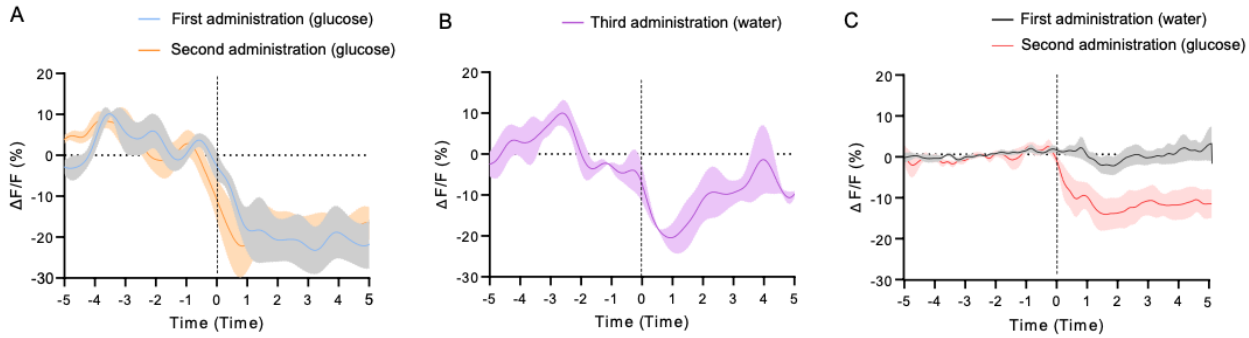

Supplementary Figure S1. AgRP neurons exhibit anticipatory responses to glucose administration via OG. (A) Mean AgRP neuron responses to the first and second OG glucose (2g/kg) (n = 3). (B) Mean AgRP neuron activity when water was administered after prior glucose exposures (n = 3). (C) AgRP neuron activity when water was given as the first OG, followed by 2.0 g/kg glucose on the subsequent gavage (n = 1).

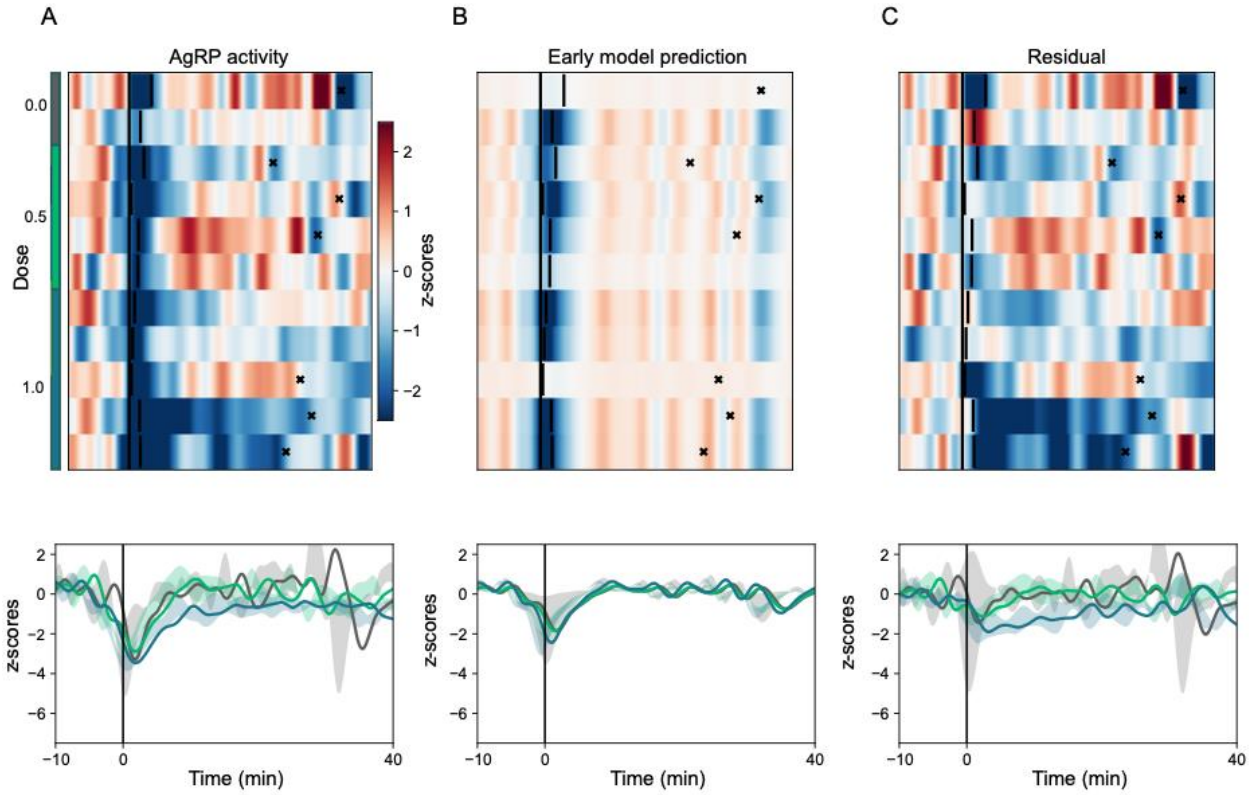

Supplementary Figure S2. Dissociation between phase 1 and phase 2 responses using an early-response model in low doses of glucose. (A-C), Heat-maps (top) and mean AgRP neuron activity (bottom) for the original (A), fitted (B), and residual (C) traces in mice administered with water (0.0), 0.5, or 1.0 g/kg glucose.

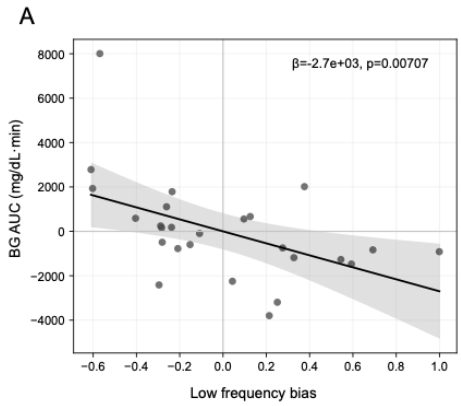

Supplementary Figure S3. Relationship between baseline low-frequency power and subsequent BG dynamics. (A), Relationship between individual session aperiodic slope in AgRP neuron activity (higher slope → greater low-frequency bias in baseline period) and incremental AUC of BG level. Slope from linear mixed effects model with corrections for OG dose and subject.

REFERENCES

[1] Mirzadeh, Z., Faber, C.L., Schwartz, M.W., 2022. Central Nervous System Control of Glucose Homeostasis: A Therapeutic Target for Type 2 Diabetes? Annu Rev Pharmacol Toxicol: 62:55-84, Doi: 10.1146/annurev-pharmtox-052220-010446.

[2] Campbell, J.E., Drucker, D.J., 2013. Pharmacology, physiology, and mechanisms of incretin hormone action. Cell Metabolism: 819–37, Doi: 10.1016/j.cmet.2013.04.008.

[3] Deacon, C.F., Ahrén, B., 2011. Physiology of incretins in health and disease. Review of Diabetic Studies: 293–306, Doi: 10.1900/RDS.2011.8.293.

[4] Skvortsova, A., Veldhuijzen, D.S., Kloosterman, I.E.M., Pacheco-López, G., Evers, A.W.M., 2021. Food anticipatory hormonal responses: A systematic review of animal and human studies. Neuroscience and Biobehavioral Reviews: 447–64, Doi: 10.1016/j.neubiorev.2021.03.030.

[5] Wachsmuth, H.R., Weninger, S.N., Duca, F.A., 2022. Role of the gut–brain axis in energy and glucose metabolism. Experimental and Molecular Medicine: 377–92, Doi: 10.1038/s12276-021-00677-w.

[6] Schwartz, G.J., 2000. The Role of Gastrointestinal Vagal Afferents in the Control of Food Intake: Current Prospects. Nutrition, Doi: 10.1016/s0899-9007(00)00464-0.

[7] Deem, J.D., Faber, C.L., Morton, G.J., 2022. AgRP neurons: Regulators of feeding, energy expenditure, and behavior. FEBS Journal: 2362–81, Doi: 10.1111/febs.16176.

[8] Hahn, T.M., Breininger, J.F., Baskin, D.G., Schwartz, M.W., 1998. Coexpression of Agrp and NPY in fasting-activated hypothalamic neurons. Nat Neurosci 1, 271–272, Doi: https://doi.org/10.1038/1082.

[9] Xu, J., Bartolome, C.L., Low, C.S., Yi, X., Chien, C.H., Wang, P., et al., 2018. Genetic identification of leptin neural circuits in energy and glucose homeostasis. Nature 556(7702): 505–9, Doi: 10.1038/s41586-018-0049-7.

[10] Sindelar, D.K., Mystkowski, P., Marsh, D.J., Palmiter, R.D., Schwartz, M.W., 2002. Attenuation of Diabetic Hyperphagia in Neuropeptide Y–Deficient Mice. Diabetes 51(3): 778–83, Doi: 10.2337/diabetes.51.3.778.

[11] Su, Z., Alhadeff, A.L., Betley, J.N., 2017. Nutritive, Post-ingestive Signals Are the Primary Regulators of AgRP Neuron Activity. Cell Reports 21(10): 2724–36, Doi: 10.1016/j.celrep.2017.11.036.

[12] Beutler, L.R., Chen, Y., Ahn, J.S., Lin, Y.C., Essner, R.A., Knight, Z.A., 2017. Dynamics of Gut-Brain Communication Underlying Hunger. Neuron 96(2): 461-475.e5, Doi: 10.1016/j.neuron.2017.09.043.

[13] Chen, Y., Lin, Y.C., Kuo, T.W., Knight, Z.A., 2015. Sensory Detection of Food Rapidly Modulates Arcuate Feeding Circuits. Cell 160(5): 829–41, Doi: 10.1016/j.cell.2015.01.033.

[14] Betley, J.N., Xu, S., Cao, Z.F.H., Gong, R., Magnus, C.J., Yu, Y., et al., 2015. Neurons for hunger and thirst transmit a negative-valence teaching signal. Nature 521(7551): 180–5, Doi: 10.1038/nature14416.

[15] Porniece Kumar, M., Cremer, A.L., Klemm, P., Steuernagel, L., Sundaram, S., Jais, A., et al., 2021. Insulin signalling in tanycytes gates hypothalamic insulin uptake and regulation of AgRP neuron activity. Nature Metabolism 3(12): 1662–79, Doi: 10.1038/s42255-021-00499-0.

[16] Goldstein, N., Mcknight, A.D., Carty, J.R.E., Arnold, M., Betley, J.N., Alhadeff, A.L., 2021. Hypothalamic detection of macronutrients via multiple gut-brain pathways. Cell Metabolism Volume 33, Issue 3, 676 - 687.e5, Doi: 10.1016/j.cmet.2020.12.018.

[17] Gou, Y., Glat, M., Damian, V., Bryan, C.L., Phan, B.A., Faber, C.L., et al., 2025. AgRP neuron hyperactivity drives hyperglycemia in a mouse model of type 2 diabetes. Journal of Clinical Investigation 135(10), Doi: 10.1172/JCI189842.

[18] Xu, J., Bartolome, C.L., Low, C.S., Yi, X., Chien, C.H., Wang, P., et al., 2018. Genetic identification of leptin neural circuits in energy and glucose homeostasis. Nature 556(7702): 505–9, Doi: 10.1038/s41586-018-0049-7.

[19] Havel, P.J., Hahn, T.M., Sindelar, D.K., Baskin, D.G., Dallman, M.F., Weigle, D.S., et al., 2000. Effects of streptozotocin-induced diabetes and insulin treatment on the hypothalamic melanocortin system and muscle uncoupling protein 3 expression in rats. Diabetes 49(2): 244–52, Doi: 10.2337/diabetes.49.2.244.

[20] Deem, J.D., Tingley, D., Bjerregaard, A.M., Secher, A., Chan, O., Uzo, C., et al., 2023. Identification of Hypothalamic Glucoregulatory Neurons That Sense and Respond to Changes in Glycemia. Diabetes 72(9): 1207–13, Doi: 10.2337/db23-0139.

[21] Brown, J.M., Scarlett, J.M., Schwartz, M.W., 2019. Rethinking the role of the brain in glucose homeostasis and diabetes pathogenesis. Journal of Clinical Investigation: 3035–7, Doi: 10.1172/JCI130904.

[22] Mirzadeh, Z., Faber, C., 2024. Brain Defense of Glycemia in Health and Diabetes. Diabetes 73(12): 1952–66, Doi: 10.2337/dbi24-0001.

[23] Rother, E., Könner, A.C., Brü, J.C., 2008. Neurocircuits integrating hormone and nutrient signaling in control of glucose metabolism. Am J Physiol Endocrinol Metab 294: 810–6, Doi: 10.1152/ajpendo.00685.2007.-As.

[24] Steinbusch, L., Labouèbe, G., Thorens, B., 2015. Brain glucose sensing in homeostatic and hedonic regulation. Trends in Endocrinology and Metabolism: 455–66, Doi: 10.1016/j.tem.2015.06.005.

[25] Stanley, S., Moheet, A., Seaquist, E.R., 2018. Central Mechanisms of Glucose Sensing and Counterregulation in Defense of Hypoglycemia. Endocrine Reviews: 768–88, Doi: 10.1210/er.2018-00226.

[26] Myers, M.G. Jr., Affinati, A.H., Richardson, N., Schwartz, M.W., 2021. Central Nervous system Regulation of Organismal Energy and Glucose Homeostasis. Nature Metabolism 3: 737750, Doi: 10.1038/s42255-021-00408-5.

[27] Whitef, J.D., Olchovsky, D., Kershaw, M., Berelowitz, M., 1990. Increased Hypothalamic Content of Preproneuropeptide-Y Messenger Ribonucleic Acid in Streptozotocin-Diabetic Rats*. vol. 126.

[28] Schwartz, M.W., Bukowski, T.R., Kuijper, J.L., Foster, D., Lasser, G., Prunkard, D.E., et al., 1996. Specificity of Leptin Action on Elevated Blood Glucose Levels and Hypothalamic Neuropeptide Y Gene expression in ob/ob Mice. Diabetes 45(4): 531–5, Doi: 10.2337/diab.45.4.531.

[29] Sahu, A., Sninsky, C.A., Kalra, S.P., 1997. Evidence that hypothalamic neuropeptide Y gene expression and NPY levels in the paraventricular nucleus increase before the onset of hyperphagia in experimental diabetes. vol. 755.

[30] Mountjoy, P.D., Bailey, S.J., Rutter, G.A., 2007. Inhibition by glucose or leptin of hypothalamic neurons expressing neuropeptide Y requires changes in AMP-activated protein kinase activity. Diabetologia 50(1): 168–77, Doi: 10.1007/s00125-006-0473-3.

[31] Berrios, J., Li, C., Madara, J.C., Garfield, A.S., Steger, J.S., Krashes, M.J., et al., 2021. Food cue regulation of AGRP hunger neurons guides learning. Nature 595(7869): 695–700, Doi: 10.1038/s41586-021-03729-3.

[32] Chen, W., Mehlkop, O., Scharn, A., Nolte, H., Klemm, P., Henschke, S., et al., 2023. Nutrient-sensing AgRP neurons relay control of liver autophagy during energy deprivation. Cell Metabolism 35(5): 786-806.e13, Doi: 10.1016/j.cmet.2023.03.019.

[33] Viskaitis, P., Tesmer, A.L., Liu, Z., Karnani, M.M., Arnold, M., Donegan, D., et al., 2024. Orexin neurons track temporal features of blood glucose in behaving mice. Nature Neuroscience 27(7): 1299–308, Doi: 10.1038/s41593-024-01648-w.

[34] Barrett, L.F., Simmons, W.K., 2015. Interoceptive predictions in the brain. Nature Reviews Neuroscience: 419–29, Doi: 10.1038/nrn3950.

[35] Zhang, J., Chen, D., Deming, P., Srirangarajan, T., Theriault, J.E., Kragel, P.A., et al., 2025. Cortical and subcortical mapping of the human allostatic–interoceptive system using 7 Tesla fMRI. Nature Neuroscience 28(11): 2380–91, Doi: 10.1038/s41593-025-02087-x.

[36] Tong, Q., Ye, C.P., Jones, J.E., Elmquist, J.K., Lowell, B.B., 2008. Synaptic release of GABA by AgRP neurons is required for normal regulation of energy balance. Nature Neuroscience 11(9): 998–1000, Doi: 10.1038/nn.2167.

[37] Deem, J.D., Tingley, D., Watts, C.A., Ogimoto, K., Bryan, C.L., Phan, B.A.N., et al., 2023. High-fat diet feeding disrupts the coupling of thermoregulation to energy homeostasis. Molecular Metabolism 78, Doi: 10.1016/j.molmet.2023.101835.

[38] Deem, J.D., Faber, C.L., Pedersen, C., Phan, B.A., Larsen, S.A., Ogimoto, K., et al., 2020. Cold-induced hyperphagia requires agrp neuron activation in mice. ELife 9: 1–48, Doi: 10.7554/eLife.58764.

[39] Faber, C.L., Deem, J.D., Phan, B.A., Doan, T.P., Ogimoto, K., Mirzadeh, Z., et al., 2021. Leptin receptor neurons in the dorsomedial hypothalamus regulate diurnal patterns of feeding, locomotion, and metabolism. ELife 10: 1–14, Doi: 10.7554/eLife.63671.

[40] Evers, S.S., Kim, K.S., Bozadjieva, N., Lewis, A.G., Farris, D., Sorensen, M.J., et al., 2020. Continuous glucose monitoring reveals glycemic variability and hypoglycemia after vertical sleeve gastrectomy in rats. Molecular Metabolism 32: 148–59, Doi: 10.1016/j.molmet.2019.12.011.